ACS APPLIED MATERIALS & INTERFACES

Research Article

www.acsami.org

Comparison of Tetragonal and Cubic Tin as Anode for Mg Ion Batteries

Zhiguo Wang,*[,†,‡] Qiulei Su,[§] Jianjian Shi,[†,‡] Huiqiu Deng,[§] G. Q. Yin,[‡] J. Guan,[‡] M. P. Wu,[‡] Y. L. Zhou,[‡] H. L. Lou,[‡] and Y. Q. Fu*[,∥]

[†]School of Physical Electronics, University of Electronic Science and Technology of China, Chengdu, Sichuan 610054, P. R. China

[‡]Joint Laboratory of Police Equipment of UESTC, Chengdu, Sichuan 610054, P. R. China

[§]Department of Applied Physics, Hunan University, Changsha, Hunan 410082, P. R. China

[∥]Thin Film Centre, Scottish Universities Physics Alliance (SUPA), University of the West of Scotland, Paisley PA1 2BE, United Kingdom

ABSTRACT: Using first-principles calculation based on density functional theory, diffusion of Mg atom into α- and β-Sn was investigated. The diffusion barriers are 0.395 and 0.435 eV for an isolated Mg atom in the α- and β-Sn, respectively. However, the diffusion barriers of the Mg atom decrease in the α-Sn, whereas they increase in the β-Sn, when an additional Mg atom was inserted near the original diffusing Mg atom, which is mainly due to strong binding of Mg−Mg atoms in the β-Sn. Therefore, it is better to use the α-Sn, rather than the β-Sn, as an anode material for Mg ion batteries.

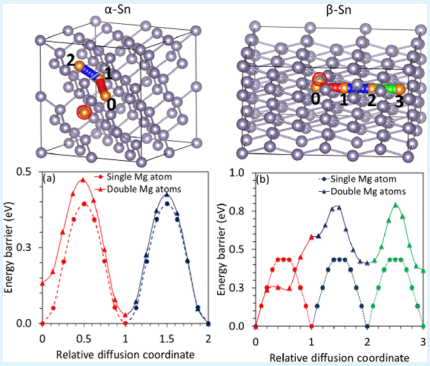

KEYWORDS: *Mg ion batteries, anode materials, density functional theory, tin, diffusion batteries, Mg−Mg interaction*

1. INTRODUCTION

Electrochemical energy storage devices such as rechargeable batteries are key components for large-scale high-power systems such as plug-in hybrid electric vehicle (PHEV) or plug-in electric vehicle (PEV). For these applications, a high-capacity anode and a high-voltage cathode are generally desirable. Rechargeable magnesium ion batteries (MIBs) are emerging as a viable next-generation technology for reversible electrochemical energy storage and conversion.[1] A magnesium ion in the MIBs carries two electrical charges (unlike the single charge of a lithium ion), thus possibly resulting in a higher theoretical volumetric energy density. The MIBs have other benefits compared with the conventional lithium ion batteries (LIBs), such as a high theoretical specific capacity (2205 $mAhg^{-1}$), abundance in the raw material, and operational safety.[2] Despite these attractive aspects of the MIBs, there are several challenges associated with uses of cathodes, electrolytes, and anodes materials in the MIBs.[2] In comparison to the LIBs, the major obstacles for the MIBs are the kinetically sluggish intercalation/insertion of Mg ions and their low diffusion in electrode materials. The search for suitable electrode materials with a fast and reversible insertion of magnesium ions still remains a major challenge.[3] Magnesium manganese silicate,[4] manganese dioxides,[5] graphene-like V_2O_5,[6] and MoS_2[7,8] were investigated as high energy density electronde materials for the MIBs. Metallic Mg can be used as anodes for the MIBs as Mg does not have the problem of dentrite formation which plagues the successful application of metallic Li anode in the LIBs. However, the MIBs using the Mg anodes[9,10] show a poor cycling ability for the reactions between the Mg anode and electrolye, due to the easy formation of a blocking layer.[2] Currently, research for novel anode materials for the MIBs is urgently needed.

Among various anode candidates, Bi, Sb, and $Bi_{1-x}Sb_x$ have been tested and results showed that Bi can be used as the anode with the conventional electrolyte.[11,12] Recently, Sn has also been investigated as the anode, and results showed that the Sn display superior operating voltages and capacity for the rechargeable MIBs.[13,14] Sn has two allotropic forms at various conditions. At the ambient pressure, the stable phase at a temperature lower than transformation temperature, T_c, of 13 °C is α-Sn (gray tin), a zero-gap semiconductor with a diamond structure. When the temperature is raised above T_c of 13°C, the Sn crystal transforms into β phase (white tin), a body centered tetragonal metal (tetragonal).[15] It is noted that the β-Sn can be changed into α-Sn upon delithiation, and the α-Sn in a polymorph remains stable at room temperature.[16] The α-Sn appearance is attributed to the nano-size effect.[16] So far, the transformation between α-Sn and β-Sn has not been reported when the Sn is used as anode for the MIBs. It is necessary to

Received: January 25, 2014
Accepted: April 2, 2014
Published: April 2, 2014

   dx.doi.org/10.1021/am500554y | *ACS Appl. Mater. Interfaces* 2014, 6, 6786−6789

investigate the suitability of the α-Sn as an anode for the MIBs and effects of the phase transformation on the diffusion of Mg atom. Understanding the Mg diffusion in the α- and β-Sn would be useful to develop the MIBs with a high capacity density.

Computer simulation is now playing a vital role in design, prediction, and characterization of the structures and properties of novel materials such as the rechargeable electrode materials, especially at the atomic scale. First-principles calculation (*ab initio*) based on the density functional theory (DFT) has been widely used to predict the output voltage of electrode materials[17−19] and other critical properties for the LIBs, including rate capability (such as electronic[20] and ionic[21] and safety[22]). Total energy calculations were also frequently used to estimate diffusion barriers by calculating energy changes along a diffusion pathway.[6] In the present study, the DFT computations are used to investigate the diffusion of Mg in the α- and β-Sn, in order to fully understand the effect of polymorphic change on Mg storage of Sn, key information for designing the high capacity density MIBs.

2. COMPUTATION DETAILS

All the calculations were performed using the DFT calculations as implemented in the Vienna *ab initio* package (VASP)[23] with a plane wave basis set. The projector augmented wave (PAW) method[24] was used to describe electron−ion interactions, while the generalized gradient approximation using the Perdew−Burke−Ernzerhof (PBE) functional was applied to describe the electron exchange correlation. The plane wave basis was set up to an energy cut-off of 450 eV. Computations for the α- and β-Sn were based on 2 × 2×2 supercell (consisting of 64 atoms) and 3 × 3×3 supercell (consisting of 108 atoms), respectively. A 3 × 3 × 3 and 3 × 3 × 5 Monkhorst−Pack[25] mesh for the *k*-point sampling of the Brillouin zone integration was used for the α- and β-Sn, respectively. Ionic coordinates were fully relaxed until the residual forces were less than 0.02 eV/Å.

To study the Mg diffusion kinetics, energy barriers were calculated using a climbing image nudged elastic band (CI-NEB) theory.[26] The CI-NEB is an efficient method to determine the minimum energy path and saddle points between the given initial and final positions. After optimization of all degrees of freedoms for each structure, the search of transition state began with a NEB calculation, which involves a chain of images (seven in the present calculations) determined through linear interpolation from the fixed initial and final configurations.

3. RESULTS AND DISCUSSION

The calculated lattice constants of the α- and β-Sn are a = 6.654 and a = 5.935, c = 3.222 Å, respectively, which are in a good agreement with experimentally obtained values of a = 6.483[27] and a = 5.831, c = 3.184 Å.[28] Different non-equivalent positions of the Mg in the α- and β-Sn lattices have been examined. After a geometry optimization, it is observed that the tetrahedral interstitial site (T_d symmetry) is the most stable form of the interstitial Mg in the α-Sn, as shown by the green balls in Figure 1a. They have four nearest-neighbor Sn atoms and six second-nearest-neighbor Sn atoms, with Mg−Sn distances of 3.03 and 3.267 Å, respectively. This is similar to the behavior of Li[29] and Na[30] atoms in the Si lattice. The most stable position for an interstitial Mg in the β-Sn is shown by the green ball in Figure 1b, which is enclosed by five Sn atoms with a bond length of ~2.00−2.73 Å. The diffusion process consists of the Mg atoms moving from one stable position to a neighboring position by passing through a hexagonal site of the α-Sn or a rhombus interstitial site of the β-Sn, as shown by the red balls in Figure 1a,b, respectively. At the hexagonal site in the α-Sn, Mg has six nearest neighbor Sn atoms, and their configuration can be

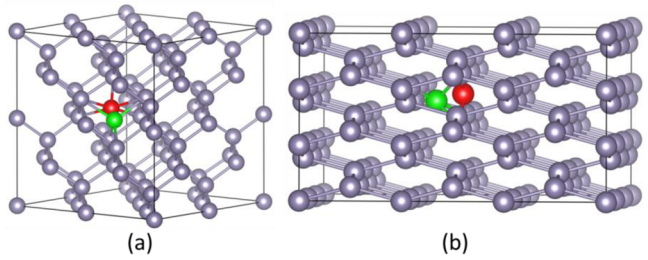

Figure 1. Atomic structures of two allotropic forms of Sn: (a) α- and (b) β-Sn. The α-Sn has a diamond structure, while the β-Sn has a tetragonal structure. The medium purple ball represents Sn atoms. Green and red balls represent the stale and transition state of Mg atoms in Sn, respectively.

viewed as two parallel triangles, both of which are perpendicular to the diffusion pathway with a Sn−Mg bond length of 2.809 Å. At the rhombus interstitial sites in the β-Sn, Mg has two nearest-neighbor Sn atoms and two second-nearest-neighbor Sn atoms, with Sn−Mg distances of 1.912 and 2.501 Å, respectively.

The energy curves for an isolated Mg diffusing between the adjacent stable sites in the α- and β-Sn are shown in Figure 2a,b

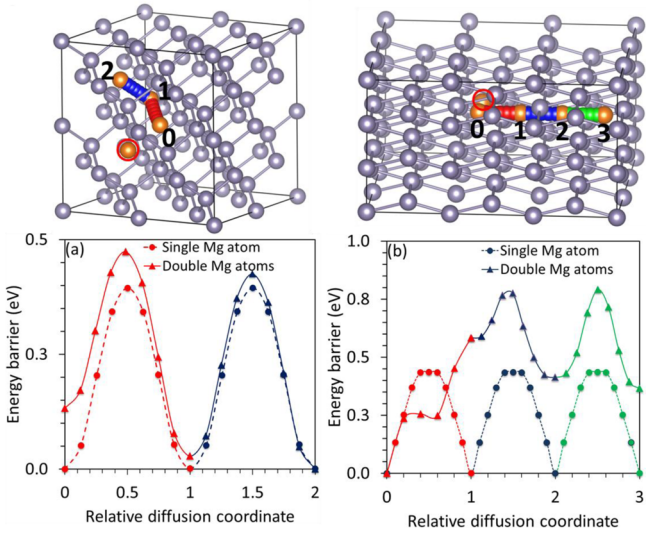

Figure 2. The energy curves for Mg diffusion between the adjacent stable sites in (a) α- and (b) β-Sn. The diffusion paths are shown above. The dashed line represents an isolated Mg diffusion, and the solid line represents the diffusion of Mg with the addition of a second Mg atom.

(the dashed line), respectively. The diffusion paths are also shown in the figures. In this case, the Mg atom marked by a red circle was not considered in the investigation in order to represent a low Mg concentration. The energy barriers are 0.395 and 0.435 eV for the Mg in the α- and β-Sn, respectively, which indicates that the Mg diffuses easily in the α- and β-Sn at a low Mg concentration. The slightly higher energy barrier for the Mg atom in the β-Sn is caused by the smaller space of the rhombus interstitial site in the β-Sn than that of the hexagonal site in the α-Sn.

Clearly, Mg atom transports easily in both of the α- and β-Sn. However, in a Mg insertion process, more Mg atoms will appear in the matrix. Therefore, we further investigated the addition of a second Mg atom (the Mg atom enclosed by a red

dx.doi.org/10.1021/am500554y | ACS Appl. Mater. Interfaces 2014, 6, 6786−6789

circle in Figure 2) and considered the Mg−Mg interaction which could change the mobility of the Mg atoms. The energy curves of the Mg atoms in the α- and β-Sn are shown in Figure 2a,b (i.e., the solid lines), respectively. Results clearly showed that the destabilization of the Sn matrix after addition of Mg atoms and the initial Mg migration caused by Mg−Mg interaction results in an asymmetrical migration pathway. It is noticed that, with the addition of a second Mg atom, the energy barrier increases from 0.43 to 0.77 eV as the Mg atoms diffuse from site 0 to site 2 in the β-Sn (as shown in Figure 2b). The addition of the second Mg atom does not affect the diffusion energy barrier of the Mg atoms from site 2 to site 3. However, in the α-Sn, the energy barrier is ~0.05 eV lower than that in the β-Sn for the Mg diffusion from site 0 to site 1. This can be viewed as an example of a cooperative diffusion, in which the diffusion occurs with a decreased energy barrier when two Mg atoms are placed closely in the low doping regime. The similar results have been reported for the Li diffusion in Si.[29] Due to the nature of the localized lattice distortions caused by the Mg insertion, the effect of Mg−Mg interaction quickly diminishes with an increase in the distance between the Mg atoms; thus, the addition of the second Mg atom does not affect the diffusion of the Mg atoms from site 1 to site 2.

To evaluate whether the Mg−Mg complexes can easily form and stably exist in the Sn lattice, we calculated the binding energy (E_b) of Mg−Mg, defined as the difference between the formation energy of the Mg−Mg (H_f(Mg−Mg)) complex and summation of each formation energy in the case of isolated Mg existing, i.e.,

$$E_b = 2H_f(\mathrm{Mg_I}) - H_f(\mathrm{Mg - Mg}) \quad (1)$$

A positive value of E_b indicates that Mg−Mg complex tend to bind each other when they are present in the samples. Figure 3

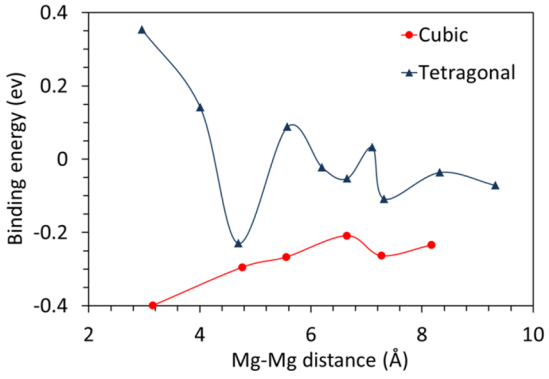

Figure 3. Binding energy of Mg−Mg complex as a function of Mg−Mg distances.

shows the calculated binding energy values as a function of Mg−Mg distance. The binding energies have negative values as the two Mg atoms are at the stable positions in the α-Sn. The binding energies decrease with increasing the Mg−Mg distance, indicating the weakening of the Mg−Mg interaction in the α-Sn. The results suggest that the Mg atoms do not tend to become clustered in the α-Sn. The destabilizing effect of the Mg−Mg will cause the decrease of the diffusion energy barrier of the Mg in the α-Sn.

However, in the β-Sn, the binding energy has a positive value of 0.354 eV when the Mg−Mg distance is about 2.96 Å, showing a dependence on the Mg−Mg distance. As the two Mg atoms appear in the β-Sn with a distance smaller than 4.0 Å, they tend to bind together. This result agrees with the above obtained dynamic results of the diffusion process, and the diffusion barrier increases with the addition of the second Mg atom in the β-Sn. We calculated the charge density differences of the Mg−Mg complex with distances of 3.15 and 2.96 Å in the α- and β-Sn, respectively, using the following equation,

$$\Delta\rho(\mathbf{r}) = \rho_{\mathrm{Mg-Mg-Sn}}(\mathbf{r}) - \rho_{\mathrm{Mg-Mg}}(\mathbf{r}) - \rho_{\mathrm{Sn}}(\mathbf{r}) \quad (2)$$

where $\rho_{\mathrm{Mg-Mg-Sn}}(\mathbf{r})$ is the charge density of the Mg−Mg complex adsorbed α- and β-Sn system, $\rho_{\mathrm{Sn}}(\mathbf{r})$ is the charge density of the Sn, and $\rho_{\mathrm{Mg-Mg}}(\mathbf{r})$ is the charge density of complex Mg−Mg atoms located at the same position as in the Mg−Mg complex adsorbed α- and β-Sn system. Figure 4a,b

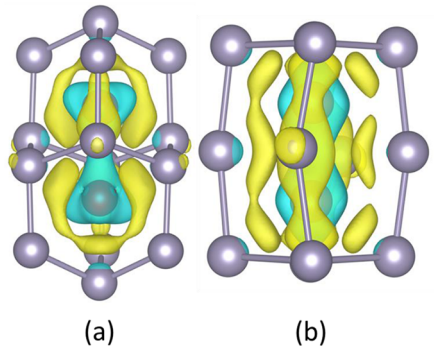

Figure 4. Isosurface of the charge density difference (0.02 e/Å^3) for Mg−Mg complex in (a) α- and (b) β-Sn. Yellow surfaces correspond to charge gains, and cyan surfaces correspond to an equivalent charge lost.

show the differences in the charge densities of the Mg−Mg complex in the α- and β-Sn, respectively. Yellow colored surfaces correspond to a gain of charges, and cyan colored surfaces correspond to a loss of equivalent charges. There is a net loss of electronic charge for each Mg atom, whereas there is a net gain of electronic charge around the Mg−Mg complex, indicating a significant difference in the charge transfer mechanisms for the single Mg atom and the Mg−Mg complex. It is noticed that the net gain of the electronic charge around the Mg−Mg complex in the β-Sn is much denser than those in the α-Sn, indicating strong binding of the Mg−Mg complex in the β-Sn.

From the above results, we can conclude that the Mg atoms are inclined to occupy the isolated stable positions in the α-Sn, which results in a homogeneous distribution. The Mg diffusion is accelerated when another Mg atom is closely positioned. However, the diffusion barrier increases with the addition of the second Mg atom in the β-Sn, which is a problem for an efficient Mg diffusion. It is much better to use the α-Sn, rather than the β-Sn, as the anode material for the MIBs.

The diffusion coefficient varies exponentially with the diffusion barrier following an Arrhenius-like formula:[31]

$$D \propto e^{-E_A/k_BT} \quad (3)$$

where E_A is the diffusion energy barrier, k_B is the Boltzmann constant, and T is the temperature. Therefore, temperatures could also affect the Mg mobility according to eq 3. However, the value of E_A is the key factor that affects the diffusion process, and a reduction of energy barrier (0.2 eV) can result in a change in the Mg mobility by a factor of ~3000 at room

temperature according to eq 3. Therefore, it needs further investigations of various processing parameters to stabilize the α-Sn by reducing the size, etc., to obtain the best performance of the Sn anode for the MIBs.

4. CONCLUSION

In summary, we performed DFT computations to investigate the possibility of using both α- and β-Sn as anode materials for the MIBs. Mg atoms prefer to be isolated in the α-Sn but form clusters in the β-Sn. The diffusion barriers of Mg atoms either decrease or increase in α- and β-Sn, respectively, when an additional Mg atom appears near the diffusing Mg atom. α-Sn is a better candidate than β-Sn to be used as an anode material for the MIBs, with high power densities and fast charge/discharge rates.

AUTHOR INFORMATION

Corresponding Authors

*E-mail: zgwang@uestc.edu.cn.

*E-mail: Richard.fu@uws.ac.uk.

Notes

The authors declare no competing financial interest.

ACKNOWLEDGMENTS

The authors thank the National Supercomputing Center in Changsha for the computing resources provided, as well as support from the Carnegie Trust Grant and Royal Society of Edinburgh in UK.

REFERENCES

(1) Novák, P.; Imhof, R.; Haas, O. Magnesium Insertion Electrodes for Rechargeable Nonaqueous Batteries - A Competitive Alternative to Lithium? *Electrochim. Acta* **1999**, *45*, 351−367.

(2) Aurbach, D.; Lu, Z.; Schechter, A.; Gofer, Y.; Gizbar, H.; Turgeman, R.; Cohen, Y.; Moshkovich, M.; Levi, E. Prototype Systems for Rechargeable Magnesium Batteries. *Nature* **2000**, *407*, 724−727.

(3) Levi, E.; Gofer, Y.; Aurbach, D. On the Way to Rechargeable Mg Batteries: The Challenge of New Cathode Materials. *Chem. Mater.* **2009**, *22*, 860−868.

(4) Nuli, Y. N.; Yang, J.; Zheng, Y. P.; Wang, J. L. Mesoporous Magnesium Manganese Silicate as a Cathode Material for Rechargeable Magnesium Batteries. *J. Inorg. Mater.* **2011**, *26*, 129−133.

(5) Rasul, S.; Suzuki, S.; Yamaguchi, S.; Miyayama, M. Manganese Oxide Octahedral Molecular Sieves as Insertion Electrodes for Rechargeable Mg Batteries. *Electrochim. Acta* **2013**, *110*, 247−252.

(6) Wang, Z. G.; Su, Q. L.; Deng, H. Q. Single-Layered V_2O_5 a Promising Cathode Material for Rechargeable Li and Mg Ion Batteries: An ab Initio Study. *Phys. Chem. Chem. Phys.* **2013**, *15*, 8705−8709.

(7) Liang, Y.; Feng, R.; Yang, S.; Ma, H.; Liang, J.; Chen, J. Rechargeable Mg Batteries with Graphene-Like MoS_2 Cathode and Ultrasmall Mg Nanoparticle Anode. *Adv. Mater.* **2011**, *23*, 640−643.

(8) Liu, Y. C.; Jiao, L. F.; Wu, Q.; Zhao, Y. P.; Cao, K. Z.; Liu, H. Q.; Wang, Y. J.; Yuan, H. T. Synthesis of GO-Supported Layered MoS_2 for High-Performance Rechargeable Mg Batteries. *Nanoscale* **2013**, *5*, 9562−9567.

(9) Ichitsubo, T.; Adachi, T.; Yagi, S.; Doi, T. Potential Positive Electrodes for High-Voltage Magnesium-Ion Batteries. *J. Mater. Chem.* **2011**, *21*, 11764−11772.

(10) Zhang, R.; Yu, X.; Nam, K.-W.; Ling, C.; Arthur, T. S.; Song, W.; Knapp, A. M.; Ehrlich, S. N.; Yang, X.-Q.; Matsui, M. alpha-MnO_2 as a Cathode Material for Rechargeable Mg Batteries. *Electrochem. Commun.* **2012**, *23*, 110−113.

(11) Arthur, T. S.; Singh, N.; Matsui, M. Electrodeposited Bi, Sb and $Bi_{1-x}Sb_x$ Alloys as Anodes for Mg-Ion Batteries. *Electrochem. Commun.* **2012**, *16*, 103−106.

(12) Shao, Y. Y.; Gu, M.; Li, X. L.; Nie, Z. M.; Zuo, P. J.; Li, G. S.; Liu, T. B.; Xiao, J.; Cheng, Y. W.; Wang, C. M.; Zhang, J. G.; Liu, J. Highly Reversible Mg Insertion in Nanostructured Bi for Mg Ion Batteries. *Nano Lett.* **2014**, *14*, 255−260.

(13) Singh, N.; Arthur, T. S.; Ling, C.; Matsui, M.; Mizuno, F. A High Energy-Density Tin Anode for Rechargeable Magnesium-Ion Batteries. *Chem. Commun.* **2013**, *49*, 149−151.

(14) Malyi, O. I.; Tan, T. L.; Manzhos, S. In Search of High Performance Anode Materials for Mg Batteries: Computational Studies of Mg in Ge, Si, and Sn. *J. Power Sources* **2013**, *233*, 341−345.

(15) Busch, G. A.; Kern, R. *Solid State Physics*; Academic: New York, 1960; Vol. *11*, p 1.

(16) Xu, L.; Kim, C.; Shukla, A. K.; Dong, A.; Mattox, T. M.; Milliron, D. J.; Cabana, J. Monodisperse Sn Nanocrystals as a Platform for the Study of Mechanical Damage during Electrochemical Reactions with Li. *Nano Lett.* **2013**, *13*, 1800−1805.

(17) Aydinol, M. K.; Kohan, A. F.; Ceder, G.; Cho, K.; Joannopoulos, J. *ab initio* Study of Lithium Intercalation in Metal Oxides and Metal Dichalcogenides. *Phys. Rev. B* **1997**, *56*, 1354−1365.

(18) Zhou, F.; Cococcioni, M.; Kang, K.; Ceder, G. The Li Intercalation Potential of $LiMPO_4$ and $LiMSiO_4$ Olivines with M = Fe, Mn, Co, Ni. *Electrochem. Commun.* **2004**, *6*, 1144−1148.

(19) Arroyo-de Dompablo, M. E.; Armand, M.; Tarascon, J. M.; Amador, U. On-Demand Design of Polyoxianionic Cathode Materials Based on Electronegativity Correlations: An Exploration of the Li_2MSiO_4 system (M = Fe, Mn, Co, Ni). *Electrochem. Commun.* **2006**, *8*, 1292−1298.

(20) Maxisch, T.; Zhou, F.; Ceder, G. Ab initio Study of the Migration of Small Polarons in Olivine Li_xFePO_4 and their Association with Lithium Ions and Vacancies. *Phys. Rev. B* **2006**, 73.

(21) Morgan, D.; Van der Ven, A.; Ceder, G. Li Conductivity in Li_xMPO_4 (M = Mn, Fe, Co, Ni) Olivine Materials. *Electrochem. Solid State Lett.* **2004**, *7*, A30−A32.

(22) Ong, S. P.; Jain, A.; Hautier, G.; Kang, B.; Ceder, G. Thermal Stabilities of Delithiated Olivine MPO_4 (M = Fe, Mn) Cathodes Investigated Using First Principles Calculations. *Electrochem. Commun.* **2010**, *12*, 427−430.

(23) Kresse, G.; Furthmuller, J. Efficiency of ab-initio Total Energy Calculations for Metals and Semiconductors Using a Plane-Wave Basis Set. *Comput. Mater. Sci.* **1996**, *6*, 15−50.

(24) Kresse, G.; Joubert, D. From Ultrasoft Pseudopotentials to the Projector Augmented-Wave Method. *Phys. Rev. B* **1999**, *59*, 1758−1775.

(25) Pack, J. D.; Monkhorst, H. J. Special Points for Brillouin-Zone Intergations - Reply. *Phys. Rev. B* **1977**, *16*, 1748−1749.

(26) Henkelman, G.; Uberuaga, B. P.; Jonsson, H. A Climbing Image Nudged Elastic Band Method for Finding Saddle Points and Minimum Energy Paths. *J. Chem. Phys.* **2000**, *113*, 9901−9904.

(27) Price, D. L.; Rowe, J. M. The Crystal Dynamics of Grey (α) tin at 90 K. *Solid State Commun.* **1969**, *7*, 1433−1438.

(28) Barrett, C. S.; Massalski, T. B. *Structure of Metals*; New York, McGraw-Hill: 1966.

(29) Wan, W.; Zhang, Q.; Cui, Y.; Wang, E. First Principles Study of Lithium Insertion in Bulk Silicon. *J. Phys.:Condens. Matter* **2010**, *22*, 41501.

(30) Malyi, O. I.; Tan, T. L.; Manzhos, S. A Comparative Computational Study of Structures, Diffusion, and Dopant Interactions between Li and Na Insertion into Si. *Appl. Phys. Express* **2013**, *6*, 027301.

(31) Janz, G. J.; Kerbs, U.; Siegenthaler, H. Molten Salts: Nitrates, Nitrites, and Mixtures: Electrical Conductance, Density, Viscosity, and Surface Tension Data. *J. Phys. Chem. Ref. Data* **1972**, *1*, 581−746.